

Figure Content Analysis for Improved Biomedical Article Retrieval

Daekeun You^a, Emilia Apostolova^b, Sameer Antani, Dina Demner-Fushman,
George R. Thoma

National Library of Medicine, National Institutes of Health, Bethesda, MD 20894

^a Dept. of Computer Science and Engineering, The State University of New York, Buffalo, NY 14260

^b College of Computing and Digital Media, DePaul University, Chicago, IL 60604

Abstract

Biomedical images are invaluable in medical education and establishing clinical diagnosis. Clinical decision support (CDS) can be improved by combining biomedical text with automatically annotated images extracted from relevant biomedical publications. In a previous study we reported 76.6% accuracy using supervised machine learning in automatically classifying images, by combining figure captions and image content to find clinical evidence. Image content extraction is traditionally applied on entire images or on pre-determined image regions. Figure images in articles vary greatly in modality and content, which limits the benefit of whole image extraction beyond gross categorization for CDS. However, image text and overlaid annotations identify the regions of interest (ROI) on the image that are referenced in the caption or discussion in the article text. We have previously reported 72.02% accuracy in text and symbols localization but in that experiment we did not exploit the referenced image locality.

In this work we combine article text analysis and figure image analysis for localizing pointers (arrows, symbols) to extract ROI pointed that can then be used to obtain meaningful image content and associate it with the identified biomedical concepts for improved (text and image) content-based retrieval of biomedical articles. Biomedical concepts are identified using National Library of Medicine's Unified Medical Language System[®] (UMLS) Metathesaurus. Our methods report an average precision and recall of 92.3% and 75.3%, respectively on identifying pointing symbols in images from a randomly selected image subset made available through the ImageCLEF 2008 campaign.

Keywords: Biomedical image analysis, biomedical article retrieval, content-based image retrieval, image overlay extraction, pointer symbol extraction, clinical decision support, natural language processing, figure caption text analysis

1. Introduction and background

Clinicians and medical researchers routinely use online databases such as MEDLINE[®] to search for bibliographic citations that are relevant to a clinical situation. They can fairly accurately form an opinion about the relevance of a publication to the clinical situation based on its title alone; however the title is not always sufficient in determining the usefulness of a publication for evidence-based practice (henceforth evidence-based utility or clinical utility)^{1,2}. Essential information is often conveyed in illustrations in biomedical publications. These images can be used to illuminate document summaries and answers to clinical questions, to enrich large image collections with textual information from articles, and for instructional purposes. The problem, however, is to automatically determine which of the images in an article will best serve each of the aforementioned purposes. At present, images needed for instructional purposes or clinical decision support (CDS) appear in specialized databases or in biomedical publications and are not meaningfully retrievable using primarily text-based retrieval systems. Our goal is to automatically annotate images extracted from scientific publications with respect to their usefulness for CDS. A future clinical decision support system (CDSS) could then provide images relevant to a clinical query or to queries for special cases important in educational settings. An important step toward attaining the goal is automatically annotating images and related text. Our approach to automatic image indexing is to describe (or annotate) an image at three levels of granularity²:

- **coarse**, which addresses
 - image modality,
 - relation to a specific clinical task (image utility),

- body location;
- **medium**, which provides a more detailed description of the image using biomedical domain ontologies;
- **specific**, which provides very detailed descriptions of clinical entities and events in an image using terms that are not included in existing ontologies, and often are familiar only to clinicians specializing in a narrow area of medicine.

In our previous exploration of coarse automatic indexing of images by modality (color image, gray-scale image, graph, graphic illustration, etc.) and image utility (suggested by the Evidence Based Medicine paradigm's six elements of a clinical scenario that an image might illustrate), we combined image and textual features in a supervised machine learning approach³. Textual features were obtained from the captions to the images and paragraphs of text containing discussion ("mentions") of these images. The text and the images were automatically extracted from the HTML-formatted articles. Text was represented as a bag-of-words or as a set of terms obtained by mapping these captions and mentions to the UMLS Metathesaurus. Texture and color features were computed on the entire image without applying any image segmentation techniques. Texture features were computed as a 3-level discrete 2-D Daubechies' discrete wavelet transform. The four most dominant colors were computed in the perceptually uniform CIE LUV color space and proved most effective. At this coarse level of granularity, a multi-class SVM classifier trained on a bag-of-words representation of image captions performed better in determining *image modality* ($84.3\% \pm 2.6\%$ accuracy) than when trained on a combination of textual and image features or features reduced to the domain specific vocabulary. For *image utility*, however, the combination of image and textual features was better than any single-source feature set achieving $76.6\% \pm 4.2\%$ accuracy.

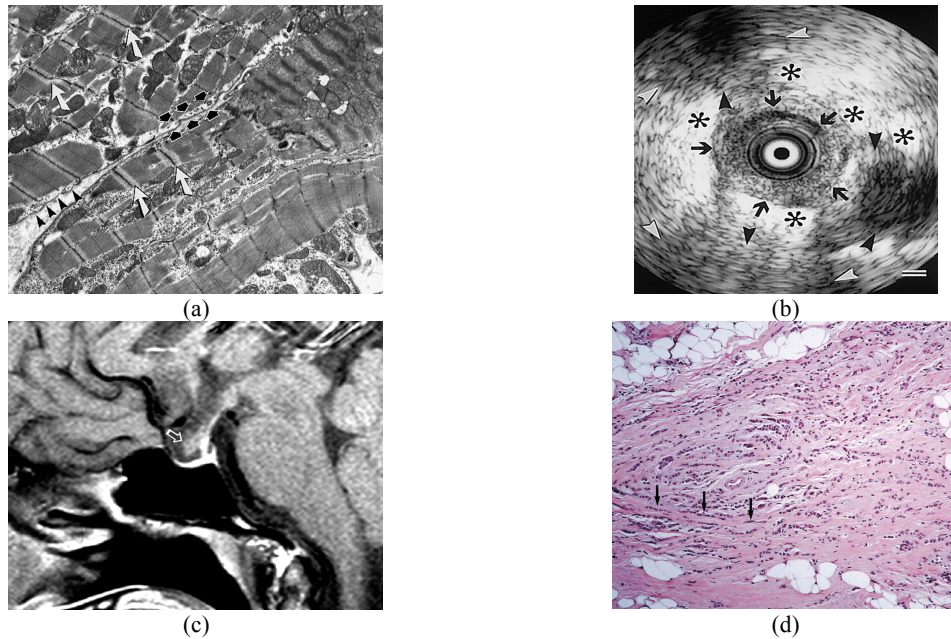


Figure 1. Examples of biomedical images with symbols

In order to compute relevance of an image to a clinical query, while it is necessary to analyze image content most approaches have traditionally relied on applying image feature extraction techniques applied on entire images or on pre-determined regions on images. Whole image analysis approaches are often unsuccessful or limited in capturing content-semantics in figure images in articles due to the large variety of images in the published literature. Locally relevant information can be gathered by extracting author-provided image-text overlays that are used to indicate regions of interest (ROI). Authors also often put several other forms of annotations on images that include pointers (e.g., arrows and arrowheads), symbols (e.g., asterisk), solid and dashed lines that are typically used to identify image ROIs in the image. Extracting these symbols may assist in measuring locally relevant image features for effective (and possibly semantically relevant) content-based image retrieval (CBIR). In previous research we have reported an accuracy of 72.02% in localization of text and symbols on extracted panel images⁴.

The challenges to reliable automatic pointer symbol localization in biomedical images are the large variety of symbol shapes, arbitrary sizes and locations, low image quality, and interference due to image background. We have developed an algorithm for extracting symbols and ROIs from biomedical images using edge-based segmentation scheme⁵ and Dynamic Time Warping⁶ (DTW) that addresses some of the problems. Figure 1 shows some sample images where image in (a) has very complex background and the background interferes the symbol boundaries; (b) shows an image which has several different shapes of symbols; (c) has only one small arrow; and (d) shows an example of a color image.

Since image annotations are also mentioned in the caption text or figure discussions in the article, we approach the problem by combining results from (i) analysis of caption and other text using natural language processing methods, and (ii) extracting pointers (arrows and other annotation symbols) from figure images by adopting document image analysis and image processing methods. Biomedical concepts in extracted snippets of text pertaining to images in scientific biomedical articles (image captions and relevant discussion in the text) are identified using National Library of Medicine's Unified Medical Language System[®] (UMLS) Metathesaurus⁷. Localizing pointers, arrows, and other annotation symbols helps identify image regions of interest that closely related to the concepts identified in the text. Resulting image features measurements can be utilized for improved (text and image) content-based retrieval of biomedical articles.

The remainder of the article is organized as follows. Section 2 describes the methods. Section 3 presents the results and discussion. Section 4 lists the challenges and conclusions.

2. Methods

A challenge in information retrieval is finding specific information with high precision and sufficient recall. Our approach to retrieve biomedical articles using a combination of image and text features is based on supervised machine learning of text and image feature matching methods.

2.1 Data

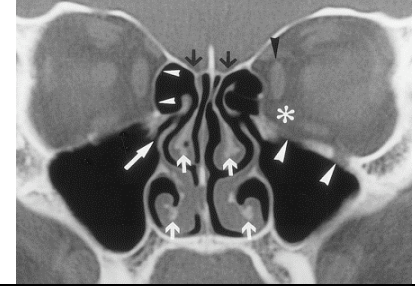
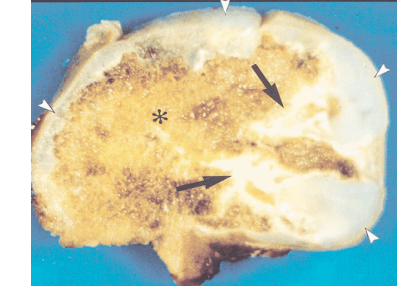
The data set for this experiment was obtained from *Radiology* and *Radiographics* journals published by the Radiological Society of North America (RSNA) made available through the ImageCLEF¹ campaign⁸. The data set has over 5,000 articles containing over 67,000 images. A coarse categorization indicated that a large proportion (approximately 50,500) images are grayscale and potentially radiological. Other illustrations (e.g., line diagrams) and color images are approximately 7,500 and 9,000 in number, respectively.

2.2 Text Snippet Processing

As indicated earlier, extracting and processing snippets of text relevant to images, such as captions and lines of text surrounding the discussion of a figure in a paragraph (mentions), can greatly assist in improving retrieval accuracy. The HTML formatting of the articles in the dataset is relatively uniform and well structured, which allowed use of regular expressions to extract figure captions and mentions. An algorithm was developed using heuristics and regular expressions to extract the caption text relevant only to the current image with an accuracy of 92%.

Many images in the dataset contain pointers that are referred to in the caption and used as an overlay in the image. Examples of such pointers include arrows, lines, and letters as shown in Figure 2. Identifying such image pointers can facilitate two goals: (i) facilitate image feature processing by identifying the type of overlay present on the image; and (ii) be the first step towards extracting the finding emphasized by these image pointers, which is usually the main concept identifying this image for annotation purposes. An algorithm was developed to extract automatically image pointers from the caption text using untrained data by providing "seed phrases" (e.g. small white arrows, arrowheads) and simple heuristics. The results were validated against 100 randomly selected captions and achieved an F-score of 0.81. An algorithm was also developed to locate *noun phrase* that was closest to the image pointer discussion in the text and proved to be accurate in predicting the image phrase referent in 68% cases.

¹ <http://www.imageclef.org>

	<p>Images obtained in a 36-year-old woman with planned heart valve implantation who was examined for inflammatory paranasal disease. (a) CT scan depicts the anatomy of the infundibular (large white arrow) and parainfundibular complex very well. The bone structures of the inferior and middle conchae (small white arrows), the orbital lamina (small white arrowheads), the orbital floor (large white arrowheads), and the cribriform lamina (black arrows) are clearly delineated. Contrast between orbital fat (*) and the medial rectus muscle (black arrowhead) is moderate. Inflammatory disease is not present.</p>
	<p>Resected solitary benign osteochondroma. (a, b) Photographs of coronally sectioned gross specimen (a) and coronally sectioned whole mount specimen (hematoxylin-eosin [H-E] stain) (b) show yellow marrow in the lesion (*) and blue hyaline cartilage cap (arrowheads). There is undulation of the hyaline cartilage that invaginates in several areas into the medullary component (straight arrows) of the osteochondroma. (c) Photomicrograph (original magnification, x250; H-E stain) reveals yellow marrow (*) and trabeculae (straight arrows) within the osteochondroma, the hyaline cartilage cap with columns of cartilage cells (arrowheads), and fibrous capsule or perichondrium (curved arrows in b and c).</p>
<p>Figure 2. Examples of image captions indicating presence of pointers and symbols (shown bold for clarity)</p>	

2.3 Pointer Detection: Pre-Processing

As indicated previously, we have coarsely divided images into three categories, viz., illustrations, grayscale images, and color images. For initial experiments we are considering only color and gray scale images. This is for the following practical reasons:

- (i) Illustrations tend to have relatively low diagnostic illustrative utility. In that sense, they offer little to compute for CBIR purposes. They may have high instructional value, however. Also, recognizing text on such images could be very valuable.
- (ii) It is relatively easy to segment lines and pointers from the background in illustrations, although it is challenging to identify which lines are truly pointers in a line diagram.
- (iii) There are more color and grayscale images in the data set.

Figure 3 shows structure of the proposed pointer symbol localization algorithm. The edge detection, edge image binarization, and contour detection are explained together as pointer symbol segmentation algorithm.

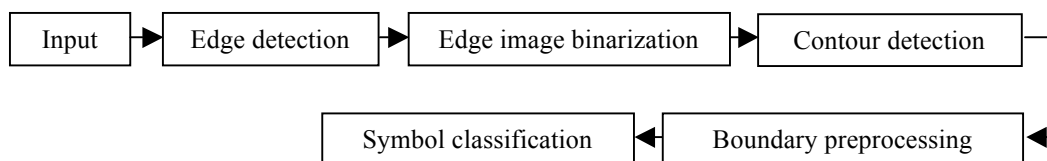


Figure 3. Schematic of the proposed pointer symbol localization algorithm

Pre-processing: The method operates on a 8-bit gray scale images. Color images are converted to 8-bit gray scale images using Eq. (1) where R, G, and B are Red, Green, and Blue channels, respectively, before it is processed for symbol localization.

$$\text{gray level intensity} = (R \times 0.306 + G \times 0.601 + B \times 0.117) \quad (1)$$

Edge detection is performed using the Roberts operator⁵. Then boundaries are converted to 8-direction chain code

Edge detection: The first step in the proposed algorithm is edge detection. The symbols of interest are overlaid graphics on biomedical images that are aimed to show particular regions of interest to reader and are likely to be easily found and readable. We assume that the symbols are likely to have sharp edges with clear color distribution. We apply the Roberts gradient operator was selected from among many well-known edge detection methods such as Canny, Sobel, Prewitt, Laplacian⁵ for its low computational cost and reasonably equivalent performance for sharp edges. The method is to be sensitive to noise.

Edge image binarization: 256-level edge images are binarized using an adaptive threshold method. Two binarization methods: Otsu⁹, and Kittler and Illingworth¹⁰ are used to calculate global and local thresholds. The global threshold is computed from the whole image and the local threshold is computed from each 64*64 sub-image. An average of the global and local thresholds is used to binarize subimages. Using both global and local thresholds together helps minimize noise edges that may be introduced if we used only a local threshold. Additionally, contour details that would be lost if we were to use a only global threshold are preserved after binarization.

Contour detection: In the contour detection step, all inner and outer boundaries of (black) connected components are detected by Freeman 8-direction chain code¹¹. Symbol boundaries are yet to be separated from the detected boundaries. The data resulting from this step is a set of points, one for each boundary, and may be large for images with noisy background. Boundaries smaller than 64 points are discarded on the observation that such small arrows are unlikely to be found in these images.

Boundary preprocessing: Only actual symbol boundaries would remain after the segmentation step if the image has simple and plain background. In many cases, however, we get many boundaries including some noise as well. Following boundary pre-processing steps are needed to improve localization: noise boundary removal, contour smoothing, data reduction, size normalization, symbol rotation, and boundary-points rearrangement.



Figure 4. Head and tail segments in symbols

Noise boundary removal: A boundary is removed as a noise boundary according to the similarity score obtained after applying Dynamic Time Warping algorithm that is described below. A boundary with similarity score below a fixed threshold, 0.6, is considered as a noise boundary and removed. Figure 4 shows examples of head segments and tail segments that are observed in common pointer symbols. Red lines are head segments and blue lines are tail segments.

Line-segment approximation: Line-segment approximation of a boundary has been frequently used in object recognition and character recognition¹². A set of consecutive boundary points that can be placed on a straight line are combined together and represented by a line segment. Not all symbols consist of straight lines but we can approximate those symbols with straight lines rather than many boundary points. Line segment approximation has data reduction effect and makes it easy to handle a boundary in later steps.



Figure 5. Results of line segment approximation of symbol boundary. Boundary on left of each subfigure is the original boundary and the one on the right is the line-segment approximated boundary.

Line segments are formed by examining the boundary chain code. If the same code appears repeatedly for five codes, a new line segment is created or added to a current line segment, if one exists. Some noisy contour points can be removed by deleting line segments of short length. Line segment approximation has a contour smoothing side effect. Figure 5

shows line segment approximation results. In Figure 5(b) curved lines are also well represented by straight lines though only one boundary is displayed.

Symbol boundary rotation and size normalization: The DTW-based template matching method is not size or rotation invariant. To deal with this problem a boundary is rotated by tilt angle of symbol rotation axis. Figure 6 shows results of symbol rotation. Eigen analysis was applied to obtain the rotation axis. A boundary is then rotated by smaller angle between the rotation axis and the X-axis. Rotation is done in line segment domain. It is not necessary to rotate each point in a boundary but just rotate two ending points of each line segment. Successfully rotated symbols indicate either a left or right pointing arrow. A limitation of this approach is the need for at least two arrow templates for each type of arrow according to the pointing direction after rotation; one template for a left pointing arrow and one for a right pointing arrow. This requires a rather large collection of various pointing symbols. A more generic approach needs to be developed and is under consideration. For size normalization, boundaries are normalized to fit in a 160×40 rectangle (4:1 aspect ratio) while preserving their aspect ratio.

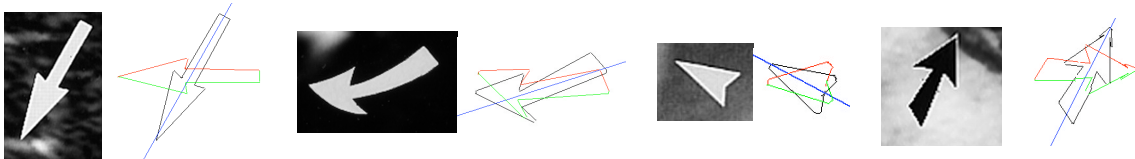


Figure 6. Symbol boundary rotation. Red and Green boundaries indicate upper and lower halves of rotated symbols. Blue line is rotation axis.

Rearranging line segments: Line segments and data points sampled from a line segments are ordered in a clockwise direction. Though the starting segment of a boundary is not important the order of sampled data points on line segments is very important since DTW compares two time series signals. To rearrange data points, all line segments are categorized into two groups (upper and lower segments) based on the rotation axis and position of the center of two ending points of each line. As shown in Figure 6 with red and green colors, if the center is above the axis, the segment is an upper line segment, otherwise it is considered as a lower segment. Data points on upper segments are rearranged by left to right order and right to left order for points on lower segments.

2.4 Pointer Detection: Symbol classification

Dynamic Time Warping (DTW) is used to compare two time series signals. It can be applied to our application since a pointer boundary is also a time series signals consisting of (x, y) points. Two boundaries, unknown and a template, are compared using DTW. More specifically, any two line segments, one from unknown and another from a template, are compared and DTW distance table is constructed. Table 1 shows a DTW matching table.

Table 1. DTW matching table

		Line segments in unknown boundary			
		seg-1	seg-2	...	seg-m
Line segments in a template	t_seg-1	dist-11	dist-12	...	dist-1m
	t_seg-2	dist-21	dist-22	...	dist-2m

	t_seg-n	dist-n1	dist-n2	...	dist-nm

Following steps describe similarity score computation for the table:

- a. Select the minimum distance from each row and column such that every segment in a set, i.e. template or unknown, matches only with one segment in the other set. In general, discard any minimum distance greater than 0.1. The threshold is determined by empirical observation.
- b. Add up the remaining distance values to get the final similarity score. Each distance is multiplied by weight value corresponding to the matched template segment. For example, if seg-2 matched with t_seg-1, and t_seg-1 is one of the two head segments in a common arrow, then, if the distance is computed as 0.0005 and the weight is 0.3, the contribution of the segment to the final similarity score is $(1-0.0005) \times 0.3 = 0.29985$.

The sum of weight values of all segments in a template is 1.0. A template giving the highest score is considered as the classification result. The total number of DTW calculations needed to classify a boundary is

$$\text{Total number of DTWs} = \sum_{T=1}^N mn_T \quad (2)$$

where N is the number of templates, n_T is the number of segments in template T, and m is the number of segments in a boundary.

2.5 Evaluation and Results

Eight commonly found symbols from our set were utilized as templates, shown in Figure 7. Their matching potential was significantly greater, however, because many other different “appearing” arrows are merely variations in aspect ratios or size of those selected.



Figure 7. Symbols in template

For evaluation three image sets, each with 100 images, were created by randomly selecting images from the data subset identified as containing some pointer or symbol by application of text analysis methods. Consequently there were no images without symbols or pointers. On average each set had 14 color images. Evaluation results are shown in Table 2. The average precision and recall are 92.3% and 75.3%, respectively. Example results are shown in Figure 8. The detected symbols are marked with red lines and extracted ROIs pointed by the arrows are displayed with red rectangles size of 100×100. It is clear from the results that the arrowheads are clearly identified and consequently the localized symbols are detected as pointing in the correct direction. Additional work is necessary on extracting more image content-based ROIs which may have non-rectangular region boundaries.

Table 2. Evaluation results

Set	True symbol detected	True symbol missed	False hit (Noise)	Precision (%)	Recall (%)
Set 1	174	53	17	91.1	76.7
Set 2	190	75	15	92.7	71.2
Set 3	192	54	14	93.2	78.0
Total/Average	Total 738 symbols			92.3	75.3

3 Discussion

The results justify the feasibility of using this method for locating biomedical image ROIs for use with further image classification, content-analysis and CBIR applications for use in CDS systems. As seen in the results the methods achieves a fairly high precision implying that the proposed DTW-based classification and localization method is appropriate for use with a known set of symbols. However, the relatively poor recall is indicative of a need for a fairly large set of templates. Examples of some unknown symbol types are show in Figure 9. We analyze various causes for the errors (false-hits and missed detections) and provide possible directions for improvements.

Errors due to weak edges: Most false hits resulted from challenging complex background images since they have more noise boundaries necessitating a more robust noise boundary removal algorithm. Improving the recall score may require: (i) modified classification algorithm; and (ii) added robustness against weak edges and broken boundaries as shown in Figure 10. Some of this problem can be addressed during the binarization step using morphological operations.

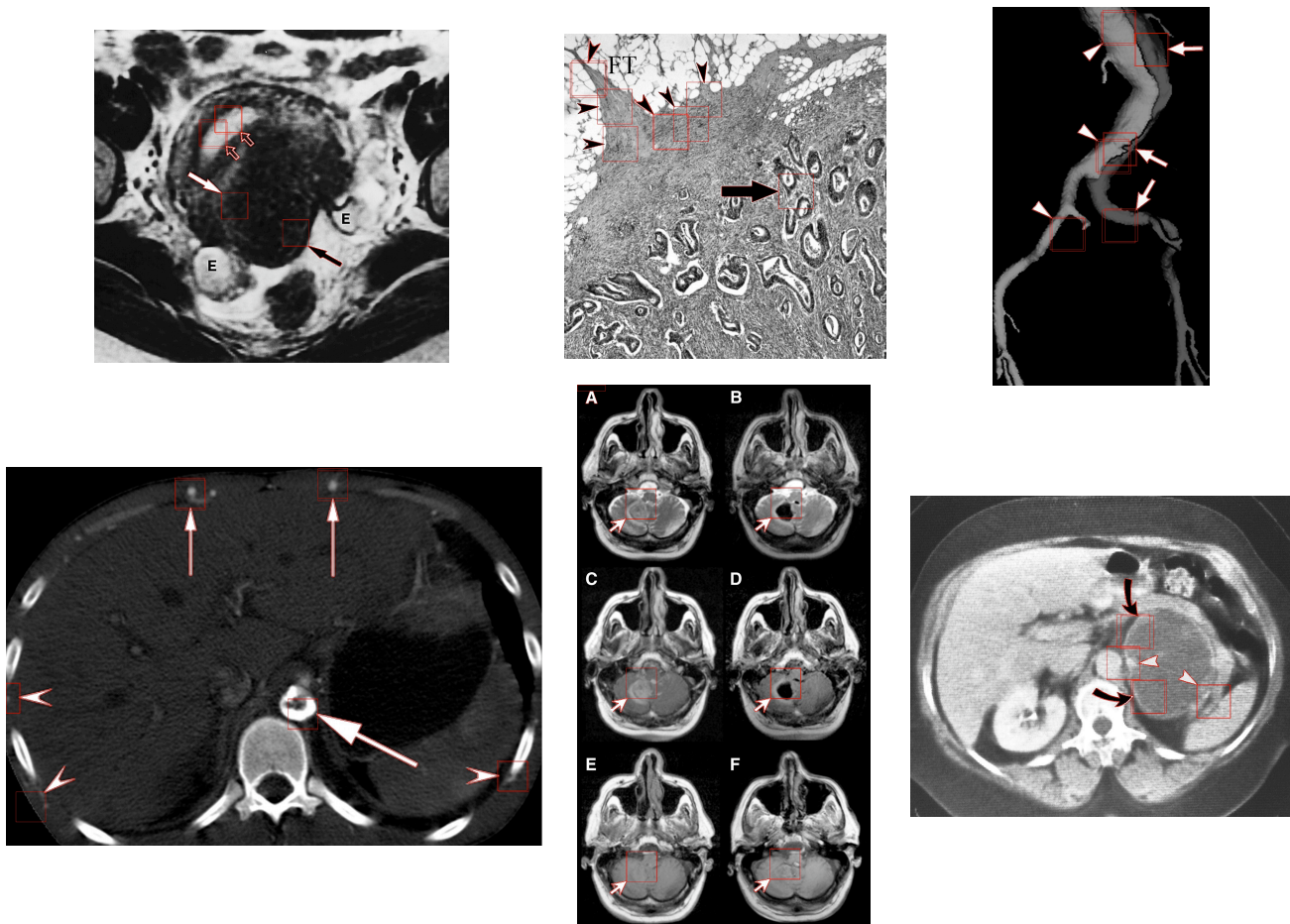


Figure 8. Symbol localization and ROI extraction results



Figure 9. Unknown symbol types

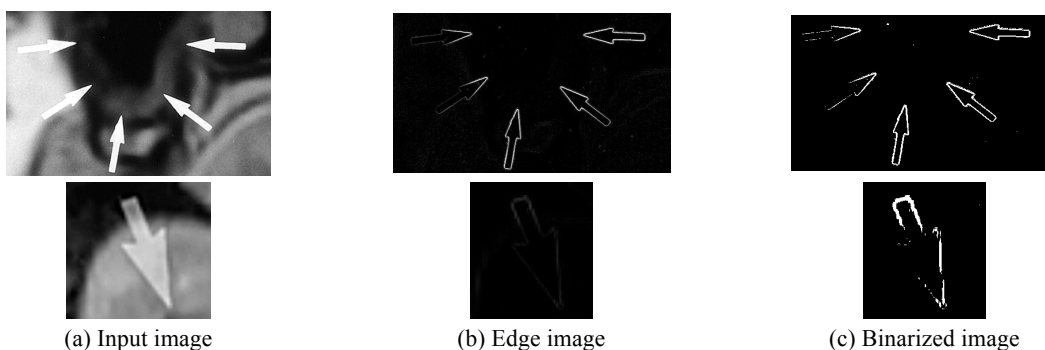


Figure 10. Symbol locating failure due to weak edge

Errors due to rotation axis computation: Main direction of a symbol can be found by Eigen analysis. The result is very accurate for most commonly occurring symbols in our data set. But for some symbols such as those with wide and/or short Eigenvector the method cannot determine the correct direction. Examples are shown in Figure 11; Figure 11(a) is a short arrow, 11(b) is a short and wide arrow, 11(c) is a bent arrow, while 11(d) is an asterisk-like symbol for

which the Eigen analysis does not work well. In many cases, we have clear edges and good line approximation results with them and alternatives to Eigen analysis could help improve results.

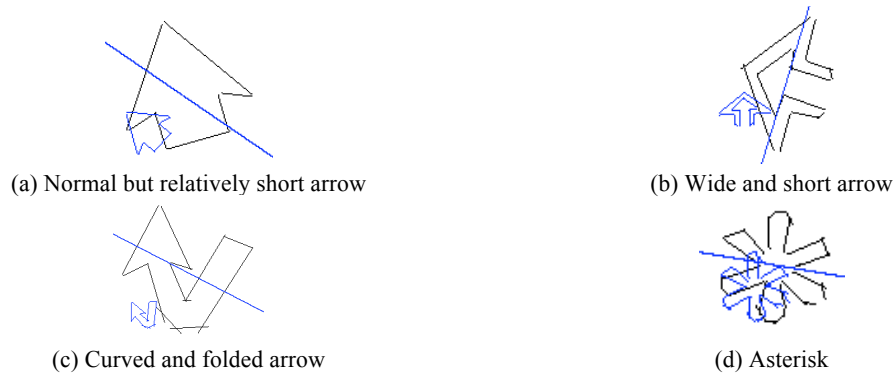


Figure 11. Failure cases of rotation axis detection. Blue arrows show resulting orientation. Blue line shows estimated rotation axis.

Errors in line segment approximation: Line segment approximation causes some problems with small symbols due to data loss. An example is shown in Figure 12 where the small part shown in the circle in a small arrow (Figure 12(a)) was not represented properly resulting the bottom half of the arrow with a different shape compared to the upper part (12(b)). This distortion causes an incorrect classification result. The lost line segment could be saved by adjusting threshold for noise segment removal or by adaptively changing the size of chain code history buffer.



Figure 12. Line segment approximation error in a small symbol

4. Conclusions and Future Work

Detecting arrows, pointers, and other annotations such as text labels, can be very beneficial in locating regions of interest within figures in biomedical articles. While existence of such annotations can be identified through relevant text snippet analysis (captions, figure mentions in the article text), image analysis methods are necessary to identify location of the symbols in the figure images. Identifying these and the image content annotated can be valuable for improved biomedical retrieval. This is achieved by attaching biomedical concepts extracted from caption and mention text analysis to image features computed at the image ROIs annotated by these symbols. Such tagging can help improve image indexing quality and subsequently the indexing and retrieval of biomedical articles through both text-based retrieval methods as well as content-based image retrieval. Both efforts can be very valuable for evidence-based practice, clinical decision support, and identifying meaningful cases for medical instruction.

In this article a comprehensive pointer-symbol locating algorithm for biomedical images has been presented. The method combines text analysis for identifying images that are likely to have some form of annotation (pointer, arrow, line, or other symbol) on them. We have developed an edge based symbol segmentation method and DTW-based symbol classification method that utilize a template library for localizing pointer and other symbols. An adaptive threshold method is applied to binarize edge image and Freeman 8-direction chain code algorithm is used to detect symbol boundaries. Several boundary pre-processing methods are implemented for improved classification results. Evaluation of the proposed algorithm on three test sets shows promising results. An average precision of 92.3% and 75.3% average recall are reported. The article presents a discussion of failure cases and proposes several techniques that may be applied to eliminate some errors. The algorithm permits localization of a fairly large and expandable set of pointer symbols. The results also show accurate localization of rectangular regions of interest pointed to by the arrows. Ongoing research

efforts aim to combine prior work in localization of other types of symbols, overlay text, and our prior work on content-based image retrieval and clinical decision support into a unified retrieval system.

Acknowledgement

This research was supported by the Intramural Research Program of the Lister Hill National Center for Biomedical Communications, an R&D division of the National Library of Medicine, at the National Institutes of Health, U.S. Department of Health and Human Services.

References

- [1] Demner-Fushman D, Hauser S, Thoma G, "The role of title, metadata and abstract in identifying clinically relevant journal articles," AMIA Annual Symposium Proceedings, 191-195 (2005).
- [2] Demner-Fushman D, Antani SK, Simpson M, Thoma GR, "Combining Medical Domain Ontological Knowledge and Low-level Image Features for Multimedia Indexing," Proc. 2nd International "Language Resources for Content-Based Image Retrieval" Workshop, OntoImage 2008, part of 6th Language Resources and Evaluation Conference (LREC 2008), (2008)
- [3] Demner-Fushman D, Antani SK, Thoma GR, "Automatically Finding Images for Clinical Decision Support," Proceedings of Workshop on Data Mining in Medicine, 7th IEEE Intl Conf on Data Mining, 139-144 (2007)
- [4] Antani S, Demner-Fushman D, Li J, Srinivasan BV, Thoma GR, "Exploring use of images in clinical articles for decision support in Evidence-Based Medicine," Proc. SPIE 6815, 68150Q1-68150Q10 (2008)
- [5] Sonka M, Hlavac V, Boyle R. [Image Processing, Analysis, and Machine Vision], Thomson-Engineering, (2007).
- [6] Martens R, Claesen L, "Dynamic programming optimisation for on-line signature verification," Proc. 4th International Conference on Document Analysis and Recognition (vol. 2), 653-656 (1997).
- [7] Aronson AR, "Effective mapping of biomedical text to the UMLS Metathesaurus: the MetaMap program," Proc AMIA Symp, 17-21 (2001)
- [8] Müller H, Kalpathy-Cramer J, Kahn Jr. CE, Hatt W, Bedrick S, Hersh W, "Overview of the ImageCLEFmed 2008 medical image retrieval task," <http://www.clef-campaign.org/2008/working%5Fnotes/CLEF2008WN-Contents1.html>, (2008)
- [9] Otsu N, "A Threshold Selection Method from Gray-Level Histograms," IEEE Trans SMC 9(1), 62-66 (1979)
- [10] Kittler J, Illingworth J, "Minimum error thresholding," Pattern Recognition 19, 41-47 (1986)
- [11] Freeman H, "On the encoding of arbitrary geometric configurations," IRE Trans Electronic Computers, 260-268, (1961).
- [12] You D, Kim G, "An approach for Locating Segmentation Points of Handwritten Digit Strings Using a Neural Network," Proc. 7th International Conference on Document Analysis and Recognition, 142-146 (2003)